Elevating solar potential of buildings with facade integration in Chinese cities

Zhe Yu,[1] Bin Ye,[1,*] Duo Lou,[1] Zhaoxuan He,[1] Zhenwei Lu,[1] Xuyang Liang,[1] Zhenzhong Zeng,[1] Jingjing Jiang,[2] and Zhiling Guo[3]
*Correspondence: yeb@sustech.edu.cn
Received: March 4, 2026; Accepted: July 2, 2026; Published Online: July 20, 2026; https://doi.org/10.59717/j.xinn-energy.2026.100179

GRAPHICAL ABSTRACT

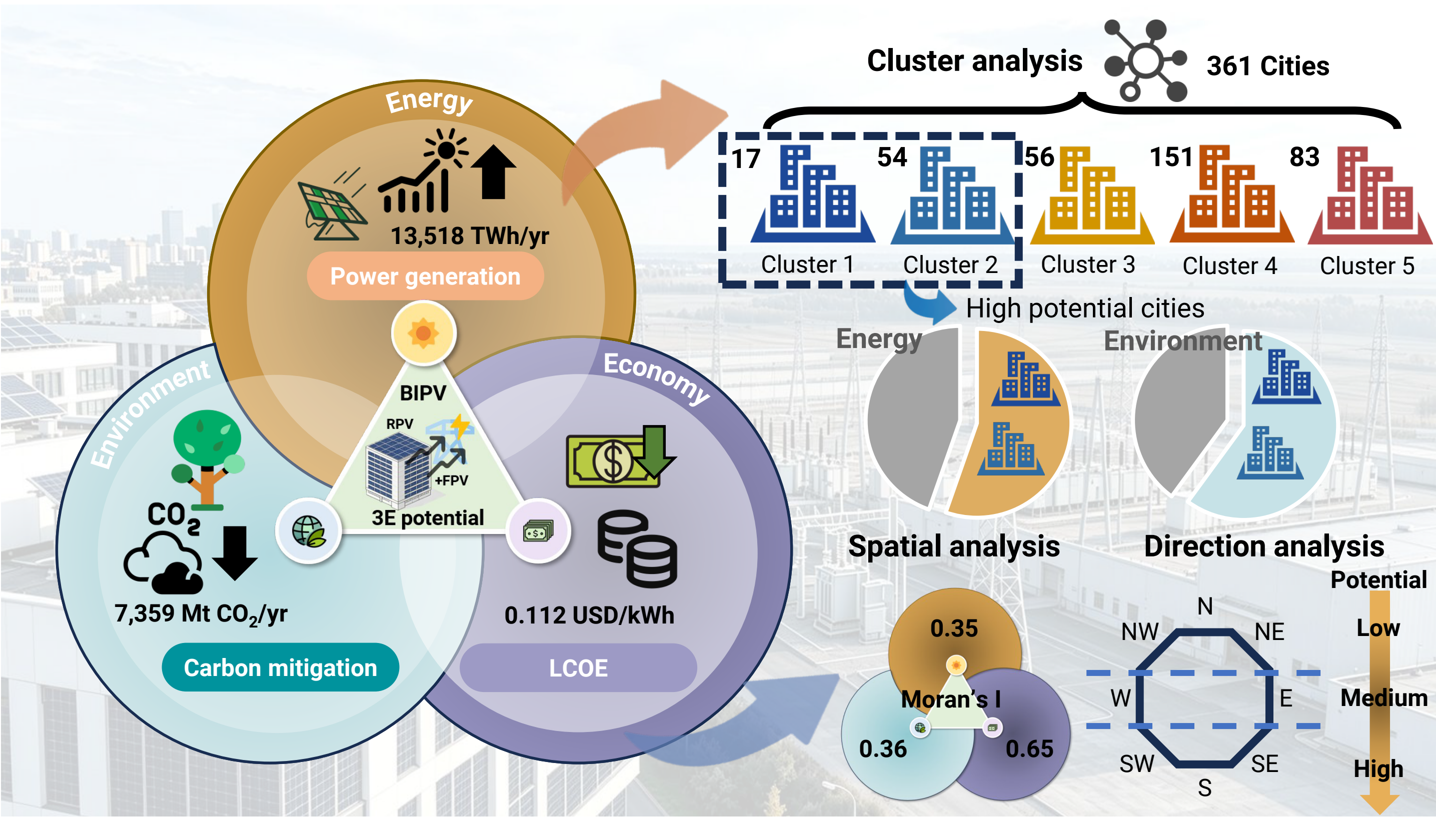

PUBLIC SUMMARY

- Building-integrated photovoltaics (BIPV) is critical for urban decarbonization, while national-scale assessments covering rooftops, multi-directional facades and urban heterogeneity are lacking.
- This study adopts 3D building data, PV_LIB model and ERA5 data to simulate BIPV output across 361 Chinese cities, achieving an annual potential of 13,518 TWh.
- Facade-integrated photovoltaics (FIPV) can boost BIPV power generation by 60% compared with rooftop-only photovoltaic systems.
- Rooftop-integrated photovoltaic (RIPV) and south-facing FIPV reduce the levelized cost of energy (LCOE) by 30%, optimizing urban BIPV economic performance.

Elevating solar potential of buildings with facade integration in Chinese cities

Zhe Yu,[1] Bin Ye,[1,*] Duo Lou,[1] Zhaoxuan He,[1] Zhenwei Lu,[1] Xuyang Liang,[1] Zhenzhong Zeng,[1] Jingjing Jiang,[2] and Zhiling Guo[3]

[1]School of Environmental Science and Engineering, Southern University of Science and Technology, Shenzhen 518055, China

[2]School of Economics and Management, Harbin Institute of Technology (Shenzhen), Shenzhen 518055, China

[3]Department of Building Environment and Energy Engineering, The Hong Kong Polytechnic University, Hong Kong SAR, China

*Correspondence: yeb@sustech.edu.cn

Received: March 4, 2026; Accepted: July 2, 2026; Published Online: July 20, 2026; https://doi.org/10.59717/j.xinn-energy.2026.100179

Citation: Yu Z., Ye B., Lou D., et al. (2026). Elevating solar potential of buildings with facade integration in Chinese cities. *The Innovation Energy* **3**:100179.

Building-integrated photovoltaics (BIPV) presents key strategy for urban decarbonization by enabling localized electricity generation on rooftops and facades. Urban building stocks offer substantial spatial potential for solar energy harvesting. However, existing studies have primarily focused on rooftop photovoltaics, and there is a lack of national-scale assessments that simultaneously consider rooftops, facades, facade orientations, and spatial heterogeneity across cities. This study integrates 3D building footprints from multi-source geospatial data to derive rooftop and facade areas, then applies the PV_LIB model with ERA5 solar irradiation data to simulate hourly generation for 361 Chinese cities. Key findings reveal an annual electricity generation potential of 13,518 TWh from building surfaces across a 159,672 km^2 target area. Notably, façade-integrated photovoltaics (FIPV) can increase the total power generation of BIPV systems by up to 60% compared with rooftop-only photovoltaic systems. To further explore the multifaceted value of this potential, this study conducts city-level spatial analysis across energy, environmental, and economic dimensions. Results from Moran's Index demonstrate that economic potential exhibits the strongest spatial autocorrelation among Chinese cities, revealing a clear north-south gradient pattern. Furthermore, an assessment of the urban photovoltaic power generation potential across different orientations reveals that rooftop-integrated photovoltaic (RIPV) and south-facing FIPV deployments optimize economic efficiency, reducing levelized cost of energy by 30%. compared with the full BIPV system. This optimization strategy enhances both energy and economic performance, offering clear guidance for BIPV planning in cities.

Introduction

Urbanization has driven an escalating demand for larger urban building scales and functional upgrades,[1,2] leading to a continued rise in urban building energy consumption.[3] Despite gradual decarbonization of energy structures, buildings in Chinese cities still account for 48.30% of national carbon emissions, which continue to increase.[4,5] In response to this trend, photovoltaic (PV) systems have recently gained prominence due to their decarbonization potential and adaptability.[6,7] By the end of 2025, China's cumulative installed PV capacity reached 1464 GW, representing 49.24% of global total.[8] However, centralized PV systems have faced significant power losses and rising costs during long-distance transmission.[9] In this context, building-integrated photovoltaics (BIPV), including rooftop-integrated photovoltaics (RIPV) and facade-integrated photovoltaics (FIPV), achieve multi-dimensional integration of energy systems and building structures by integrating PV panels as functional components of the building envelope.[10,11] Since BIPV systems can be directly installed on building surfaces, their power generation and load centers are spatially aligned, thereby effectively achieving demand-driven power generation and reduced transmission losses. More importantly, China possesses a growing building stock, with an average annual increase of 3,500 km^2 in new building area over the past decade.[12] This large-scale, continuously developing architectural resource provides unique spatial advantages. Therefore, it is urgent for China to conduct city-level BIPV potential assessments to fully leverage the spatial advantages of its vast building stock and advance its renewable energy utilization.

Despite this potential, current assessments remain limited. Current studies have demonstrated the feasibility of BIPV systems in specific urban contexts. However, they have several limitations, including the systematic neglect of facade installation potential and a narrow focus on single-city evaluations, resulting in limited reference value for broader BIPV system planning.[13,14] Previous studies have found that FIPV can increase power generation by approximately 60% compared to rooftop-only RIPV systems.[15] However, these studies only focused on China's ten largest cities, and the limited data constrained their ability to support an analysis of urban heterogeneity. Therefore, incorporating the potential of FIPV into the BIPV assessment framework addresses the research gap in the assessment of building facade resources at the urban level[16,17] and further investigates the differences in BIPV systems across cities. For a more holistic evaluation of BIPV sustainability, the multi-dimensional analysis of the energy-environment-economy (3E) factors is critical.[18,19] Considering China's administrative structure comprising more than 300 prefecture-level cities, each of which exhibits distinct spatial heterogeneity in building form,[20] solar radiation resources,[21] and economic development levels,[22] single-case studies are inadequate for supporting nationwide statistical inferences. Moreover, this study constructs a cross-regional analysis model covering China's prefecture-level cities, overcoming the scale limitations of single-city studies. By conducting statistical inference on the heterogeneity of BIPV systems at the city level, we can more accurately reveal the differences between cities and help formulate differentiated policies for BIPV systems.

Furthermore, the distinct architectural landscape of Chinese cities presents unique opportunities and challenges for BIPV deployment. This landscape is characterized by high-density development, diverse building forms ranging from low-rise to high-rise, and significant regional variations in rooftop designs and orientations.[23] Concurrently, advancements in GIS technology provide strong support for acquiring high-precision building data.[24,25] Against this backdrop, scientifically quantifying the application potential of BIPV systems urgently requires a comprehensive assessment of their energy-saving, emission-reduction benefits and investment feasibility. Such evaluations aim to optimize PV utilization efficiency in building applications, reduce the cost of PV power generation, and promote BIPV technological progress.

Three research gaps motivate this study. First, existing studies have primarily focused on rooftop photovoltaics, while systematic assessments of facade-integrated photovoltaic potential remain insufficient. Second, previous work has largely relied on case studies of a single city or a few cities, lacking a national-scale comparison across cities. Third, the literature has emphasized power generation potential, with limited attention to integrated energy-environment-economic evaluations and spatial heterogeneity analysis. To address these gaps, this study couples urban building information systems with multi-parameter dynamic models and constructs a multi-dimensional evaluation framework encompassing power generation, carbon mitigation, and levelized cost of energy (*LCOE*). Using this framework, we quantify BIPV potential for 361 prefecture-level cities. We further analyze the spatial heterogeneity of BIPV potential across these cities and employ uncertainty analysis to provide a robust quantification of current city-scale BIPV technical potential. These findings provide a scientific benchmark for differentiated regional policy designs and support future BIPV development.

MATERIALS AND METHODS

The methodological framework consists of four steps: building surface extraction, BIPV generation simulation, 3E performance assessment, and spatial heterogeneity analysis (Figure 1).

In the first step, we extract building footprints, heights, and orientations

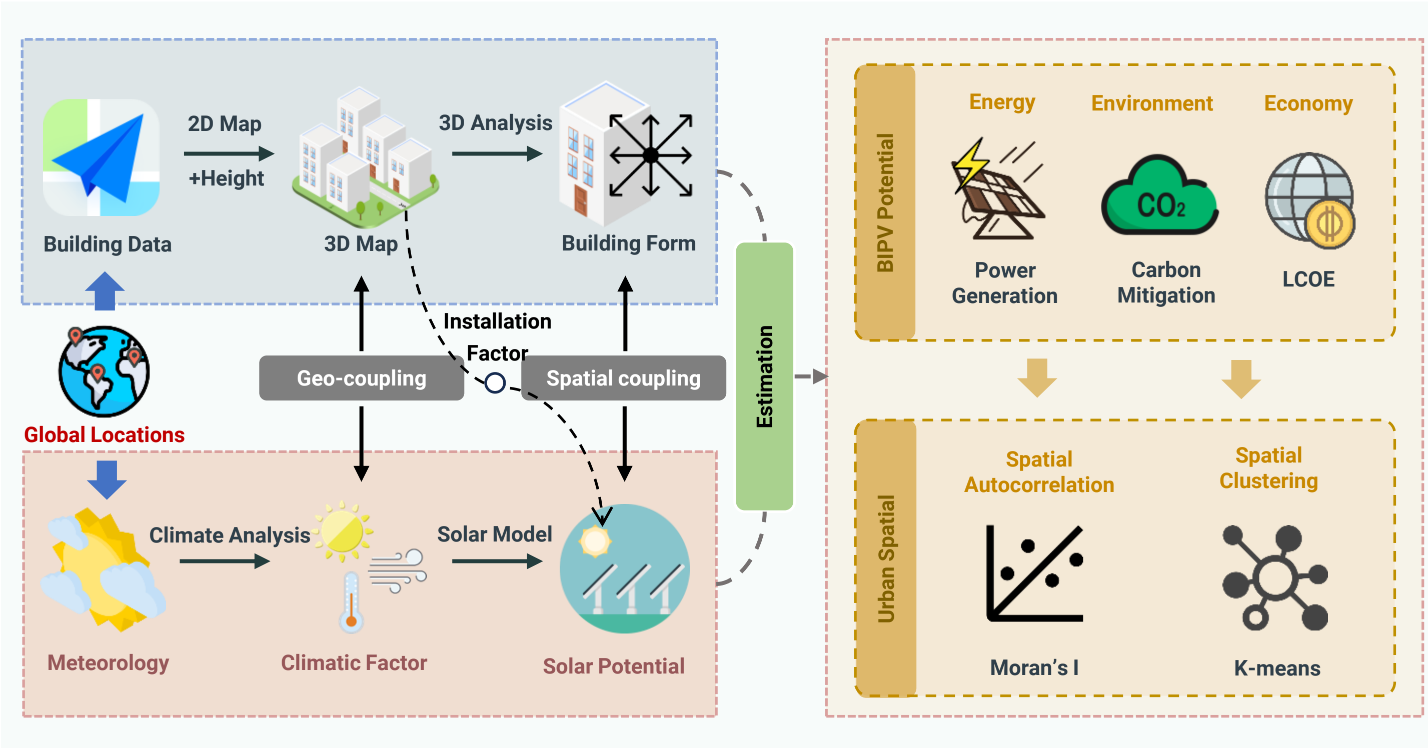

Figure 1. Framework for assessing the potential of BIPV at the city level based on geographical and environmental factors

from multi-source geospatial data to compute rooftop and facade areas for each of the 361 cities. In the second step, we simulate hourly photovoltaic generation using PV_LIB with ERA5 solar irradiation data. In the third step, we quantify carbon mitigation based on provincial grid emission factors and calculate the *LCOE* using economic parameters. In the fourth step, we perform clustering using K-means++ and spatial autocorrelation using Moran's I to reveal heterogeneity patterns across cities.

Methodological assumptions and building data

Consistent assumptions were applied for the BIPV systems analyzed in this study. Key performance parameters for PV applications were established based on current technical capabilities within the PV industry, a conservative choice to account for suboptimal tilt and higher soiling on vertical surfaces compared to tilted rooftops. These efficiency values are module-level DC efficiencies before system losses. These include a conversion efficiency of 20% for RIPV systems and 15% for FIPV modules.[14] The distinct efficiency values reflect different module technologies: rooftops use monocrystalline silicon, while façades use thin-film modules for better aesthetic and lightweight integration

According to the literature, efficiency correction factors accounting for PV module performance, solar radiation utilization, and surface contamination were incorporated. This yielded an average PV system energy efficiency ratio of 0.8, which includes temperature losses, inverter efficiency of 96%, DC/AC ratio of 1.2, cabling losses, and moderate soiling. City-specific soiling rates are not available for all 361 cities; the 0.8 Performance Ratio (PR) represents a consistent national average. This PR value is derived from the efficiency correction factors of PV systems (Table S4). Multiplying these component factors yields an overall performance ratio range of 0.75-0.85, with a mid-range value of approximately 0.8, which we adopt as the baseline. This range implicitly accounts for regional variations in soiling and other environmental conditions, with northern cities at the lower end and southern cities at the higher end. The Monte Carlo uncertainty analysis PR is varied across this full range.

The analysis also accounted for the effects of rooftop appurtenances, window openings, and building shading on facade potential. Consequently, it was assumed that 70% of building rooftops and 40% of building facades were available for installing RIPV and FIPV systems, respectively.[26,27] To assess the sensitivity of our results to these assumptions, we tested alternative coverage factors including RIPV coverage from 50% to 70% and FIPV coverage from 30% to 50% in Supplementary Table S4 The results show that national generation changes by −15% to +12%, confirming the robustness of our core findings.

The research encompasses 361 prefecture-level cities across China, representing 97% of the nation's urban data. Hong Kong, Macau, Taiwan, Tibet, and Sansha (Hainan) were excluded due to the unavailability of baseline emission factors. The building data for this study were mainly from Che et al. (2025).[28] This dataset leveraged Earth Observation (EO) data and advanced machine learning techniques to integrate multi-source remote sensing features and building morphological characteristics, thereby developing a global building height map (3D GloBFP) based on the building footprint. In addition, the AMap Building Database, which was provided by the Institute of Geographic Sciences and Nature Resources Research, Chinese Academy of Sciences (IGSNRR, CAS), serves as complementary data. This database encompasses all buildings within the primary urban and suburban areas of 361 prefecture-level cities. It amalgamates the distribution and structural attributes of diverse urban structures by leveraging Global Positioning System (GPS) technology and AI-driven building recognition algorithms and incorporates detailed building height information.

To validate our facade area estimates, we compared our 2.5D extrusion results against high-resolution 3D models from Google Earth 3D for 120 buildings across Beijing, Shanghai, and Shenzhen. The validation results show low errors. The mean absolute percentage error for total facade area is 23%, and the Spearman's rank correlation coefficient between estimated and true values is 0.91, confirming that the relative ranking of cities by facade potential is highly reliable. Orientation-specific errors are also within acceptable ranges. To further validate orientation-specific façade area estimates, we disaggregated the 120 validation buildings in Beijing, Shanghai, and Shenzhen by eight orientations (N, NE, E, SE, S, SW, W, NW). The mean absolute percentage error (MAPE) for south-facing façades is 24%, which is comparable to other orientations. Spearman's rank correlation coefficients for all orientations exceed 0.87, confirming that our 2.5D extrusion method does not introduce a systematic directional bias.

After acquiring the vector files containing building information, we processed the building footprints by converting them into lines. These lines were then segmented at their vertices. Subsequently, the length and azimuth of each line segment were calculated. This procedure enabled the derivation of both the rooftop area and the facade areas of the buildings from various angles. The resulting area data were then aggregated at the city level. We acknowledge that this 2.5D extrusion assumes all buildings are perfect vertical prisms and ignores real morphological features such as setbacks, podiums, balconies, curved facades, and irregular rooflines. This simplification may affect orientation-specific facade area estimates, particularly for south-facing facades. However, for a national-scale screening across 361 cities, the relative ranking of cities by facade potential remains robust as confirmed by validation.

Tri-aspect analysis for BIPV system

The amount of electricity generated by a BIPV system is critical for subsequent 3E potential assessments. For this purpose, we used a toolbox developed by Sandia National Laboratories (SNL) called PV_LIB to calculate the power generation of BIPV systems.[29] The solar irradiation values used in this study were obtained from the ERA5 reanalysis dataset provided by the European Centre for Medium-Range Weather Forecasts. Hourly global horizontal irradiance and direct normal irradiance are extracted at 0.25-degree spatial resolution for each city location. Climatic assumptions are based on typical meteorological year data averaged from 2010 to 2020. For the sky model we adopt the isotropic diffuse model as described by Liu and Jordan, which is the default model in PV_LIB for annual energy yield simulations. The shadows cast by high-rise buildings on neighboring structures can reduce daily PV potential by up to 17% compared to low-rise buildings, where mutual shading is less pronounced. Our simplified method may therefore overestimate generation in dense urban cores by a similar margin.

We do not perform dynamic ray-tracing for inter-building or self-shading. Instead, shading effects are implicitly incorporated through two aggregated factors. First, the 40% facade usability factor includes a deduction for shading from neighboring buildings and from building projections such as balconies and overhangs. Second, the performance ratio of 0.8 includes a loss factor of 0.96 for partial shading, based on typical values for urban BIPV systems. The 15% module conversion efficiency for FIPV does not separately account for shading. The shading effect is entirely handled by the usability factor and the performance ratio. This simplified approach does not account for detailed hour-by-hour shadow patterns. In high-density urban canyons, mutual shading can reduce actual generation by up to 38%. Our method may therefore overestimate generation in such areas by an estimated 15 to 30%. A more detailed discussion is provided in the Limitations section. Vegetation shading is completely neglected in this assessment because the GloBFP building dataset does not contain vegetation data. Vegetation shading mainly affects lower floors up to about 10m in height. In high-rise dominated districts, this omission has a minor impact on total facade potential. However, in low-rise residential neighborhoods with dense street trees, our method may modestly overestimate generation. We recommend future studies to integrate LiDAR-based vegetation canopy models for city-scale assessments. The toolbox includes modules for model selection, geographic location, and installation parameter settings, PV module and inverter configuration, temperature prediction, and power generation calculation. For rooftop systems, we assume a south-facing orientation with a tilt angle equal to the local latitude. The spacing loss is implicitly accounted for in the 70% rooftop coverage factor, which already reduces the gross roof area to a net installable area. For facade systems, modules are mounted flush with the wall, meaning vertical with tilt equal to 90 degrees, and oriented according to the wall's azimuth.

In this study, we adopt height thresholds of 10m and 27m to classify buildings into three categories. Buildings below 10m are defined as low-rise, corresponding to 1 to 3 floors. Buildings between 10m and 27m are defined as mid-rise, corresponding to 4 to 8 floors. Buildings above 27m are defined as high-rise, corresponding to 9 floors or more. This classification follows the standard Chinese building height regulations as reported by the Ministry of Housing and Urban-Rural Development of China.[30,31] Low-rise buildings are mostly single-family villas or older residential buildings. For such buildings, facade installation is relatively easy when using ladders or small lifts. Mid-rise buildings are typically multi-story apartment blocks built from the 1980s to the 2000s. Facade installation on mid-rise buildings may require scaffolding but is still feasible. High-rise buildings are modern residential or office towers. Installing FIPV on high-rise facades demands specialized equipment such as suspended platforms or drone-assisted systems, and maintenance costs are higher. These thresholds therefore reflect both the shading effect, as taller buildings cast longer shadows on neighboring structures, and the practical feasibility of FIPV installation across different building classes.[32]

Regarding balance of system components, inverter efficiency is set to 96%, typical for string inverters used in BIPV systems. We assume no module-level power optimizers because the shading analysis is simplified; this may slightly underestimate performance in partially shaded conditions. The DC to AC ratio is assumed to be 1.2. Cabling and other balance-of-system losses are included in the overall performance ratio of 0.8. A breakdown of the performance ratio components is provided in Supplementary Table S5.

To assess the environmental potential of BIPV systems, the focus is on measuring their carbon mitigation. Since the life cycle carbon emissions of the BIPV system are much smaller than the emissions prevented during the operation phase, any other life cycle phases are not considered. The baseline emission factor for each city is taken as the average carbon emission factor for electricity at the provincial level to which it belongs (Table S3). The carbon emission reduction factors of BIPV systems based on different power grids are calculated according to Equation (1):

$$BIPV_{CM} = BIPV_{PG} \times EF_C \tag{1}$$

where $BIPV_{CM}$ is the carbon mitigation of the BIPV system, $BIPV_{PG}$ is the power generation of the BIPV system, and EF_C is the average carbon emission factor for electricity.

The cost of energy for a power generation project can be evaluated by several methods, of which *LCOE* is the most common. This method is commonly used when comparing different generation technologies or evaluating grid parity for emerging technologies. *LCOE* calculates the cost of electricity generation over the entire life cycle of a PV system based on PV investment costs and operating and maintenance cost parameters (Table S3). The *LCOE* was calculated according to Equation (2):

$$BIPV_{LOPE} = \frac{I + \sum_{t=1}^{n} \frac{M_t}{(1+d)^t}}{\sum_{t=1}^{n} \frac{E_t}{(1+d)^t}} \tag{2}$$

where I is the initial investment, M_t is the operating and maintenance cost in year t, E_t is the power generation in year t, d is the discount rate, which is set to 8% based on the benchmark rate for renewable energy projects in China, and n is the project life, which is generally 25 years.

To quantify the uncertainty in our annual generation estimates, we performed a Monte Carlo simulation with 10,000 iterations. The following input parameters were simultaneously varied using triangular distributions within plausible ranges: solar irradiation, module efficiency, rooftop coverage, façade coverage, and performance ratio. These ranges are based on literature values and the sensitivity analyses presented in Supplementary Tables S4 & S5.

Clustering algorithm for 361 prefecture-level cities

To identify distinct patterns of BIPV potential across cities and to support differentiated policy recommendations, we applied K-means++ clustering to the 361 prefecture-level cities. Clustering groups cities with similar characteristics, enabling tailored deployment strategies instead of a one-size-fits-all approach.

Three variables were selected for clustering: total BIPV power generation measured in TWh per year, carbon mitigation measured in Mt CO_2 per year, and levelized cost of energy measured in USD per kWh. These variables capture the three dimensions of the 3E framework, namely energy, environment, and economy, and are the primary outputs of our assessment.

The optimal number of clusters k was determined using the elbow method combined with silhouette analysis. The elbow method plots the within-cluster sum of squares against k, and the optimal k is identified at the elbow point where the marginal gain starts to diminish. Silhouette analysis measures how similar each city is to its own cluster compared to other clusters, with higher average silhouette scores indicating better separation. Applying both methods to our dataset yielded an optimal k of 5 as the optimal number of

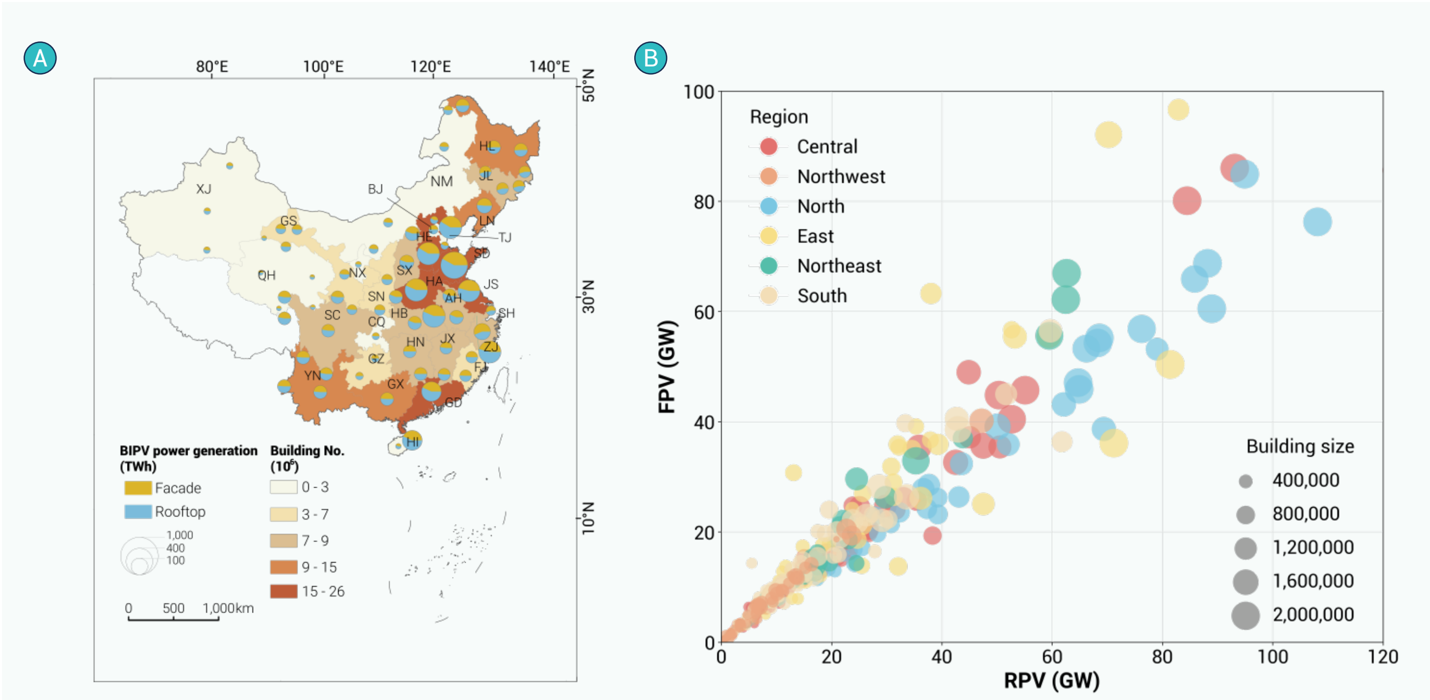

Figure 2. BIPV Power Generation at Provincial and Municipal Levels (A) Provincial-level BIPV power generation. (B) Municipal-level RIPV and FIPV power generation.

clusters.

With k set to 5, the K-means++ algorithm initializes cluster centers, assigns each city to the nearest center based on Euclidean distance in the standardized feature space, updates the centers iteratively, and converges when assignments stabilize.

Spatial heterogeneity analysis for BIPV potential

Moran's I is a core indicator used in spatial statistics to quantify spatial autocorrelation.[33] This study applies the global Moran's I and local Moran's I to conduct spatial autocorrelation tests on BIPV systems at the city-level in China, in order to determine whether there is a correlation between the observed values of different cities. Global spatial autocorrelation analysis identifies whether significant spatial clustering or outliers exist across the study area. If significant global autocorrelation is detected, we subsequently perform local spatial autocorrelation analysis. The Local Moran's I statistic pinpoints the specific locations exhibiting statistically significant spatial outliers (hot spots or cold spots) or clusters. calculated the Euclidean distance between each pair of cities, and spatial weighting was assigned using the inverse distance weighting (IDW) method. The Moran's I was calculated according to Equation (3):

$$Moran's\ I = \frac{n}{\sum_{i=1}^{n}\sum_{j=1}^{n} w_{ij}} \times \frac{\sum_{i=1}^{n}\sum_{j=1}^{n} w_{ij}(x_i-\bar{x})(x_j-\bar{x})}{\sum_{i=1}^{n}(x_i-\bar{x})^2} \qquad (3)$$

where n is number of spatial units, x_i and x_j are observed value at spatial unit i and j, $\bar{x}$ is mean of observed values, w_{ij} is spatial weight between units i and j. In this study, a confidence level of 95% was applied to determine statistical significance.

RESULTS

Power generation potential for BIPV based on building form

We estimate that there are 222 million buildings and utilize a geospatial vector dataset to quantify their rooftop and facade area. The urban building form parameters mainly include: rooftop area, facade area, and aspect ratio (Figure S1).[34] These buildings are mainly distributed southeast of the Heihe-Tengchong line in China[35]. The total areas of building rooftops and facades reached 4.49×10^4 km^2 and 1.15×10^5 km^2, respectively. The facade area in each city was about 2.48 times the rooftop area (R^2=0.945), showing a significant linear correlation (Supplementary Fig.2). These buildings generally exhibit by a "longer in the north-south direction and wider in the east-west direction" orientation. Building aspect ratios increase with latitude. This higher aspect ratio provides a significant advantage in maximizing the south-facing facade, which has the greatest potential among all orientation.

Considering the distribution of buildings nationwide, we estimate the average power generation potential of BIPV installed on building surfaces is 13,518 TWh/yr (Figure 2). The sensitivity analysis of coverage factors, presented in Supplementary Table S5, shows that varying RIPV coverage from 50% to 70% changes the national generation by -15% to 0%, while varying FIPV coverage from 30% to 50% changes it by -25% to 25%. Including facade area yields an 84% increase in power generation compared to a single RIPV system. Considering the practical constraints of PV installation on high-rise building facades, this study defines building height as a key limiting factor. When the height thresholds are set at 10m (low-rise buildings) and 27m (high-rise buildings), the installable facade area decreases by 49.30% and 83.98%, respectively. Correspondingly, the power generation potential is reduced to 10,496 TWh/yr and 8,335 TWh/yr under these two scenarios.

When a 40% coverage rate is assumed for FIPV, the installable area of building-integrated photovoltaics nationwide increases by 147% relative to the baseline scenario Although the potential of facade photovoltaics is lower than that of rooftop photovoltaics, the total national BIPV power generation increases by 84%, which can cover China's electricity demand. The Shandong province demonstrates strong power generation potential, with rooftops contributing 736.06 TWh and facades contributing 533.99 TWh, together accounting for 12% of the total national BIPV output. While Chongqing has relatively low solar radiation levels, its abundant building resources contribute to a power generation potential of 165 TWh. Provinces with an annual potential exceeding 1,000 TWh are primarily located in the eastern China: Shandong, Hebei, Henan, and Jiangsu.

Under the height constraints of 10m and 27m, which were established by considering building typologies and the feasibility of installing FIPV systems, the power generation potential still exceeds that of a standalone RIPV system by 42.8% and 13.4%, respectively. The impact of these constraints is smallest in southeastern Chinese cities, where the average building height is generally higher. In high-density urban centers like Shenzhen and Beijing, the prevalence of tall buildings offers vast vertical facade areas, presenting a significant opportunity for power generation. The substantial technical potential identified under various constraints underscores the promise of BIPV systems. To translate this promise into operationalizable strategies, however, it is imperative to evaluate the current generation potential through an inte-

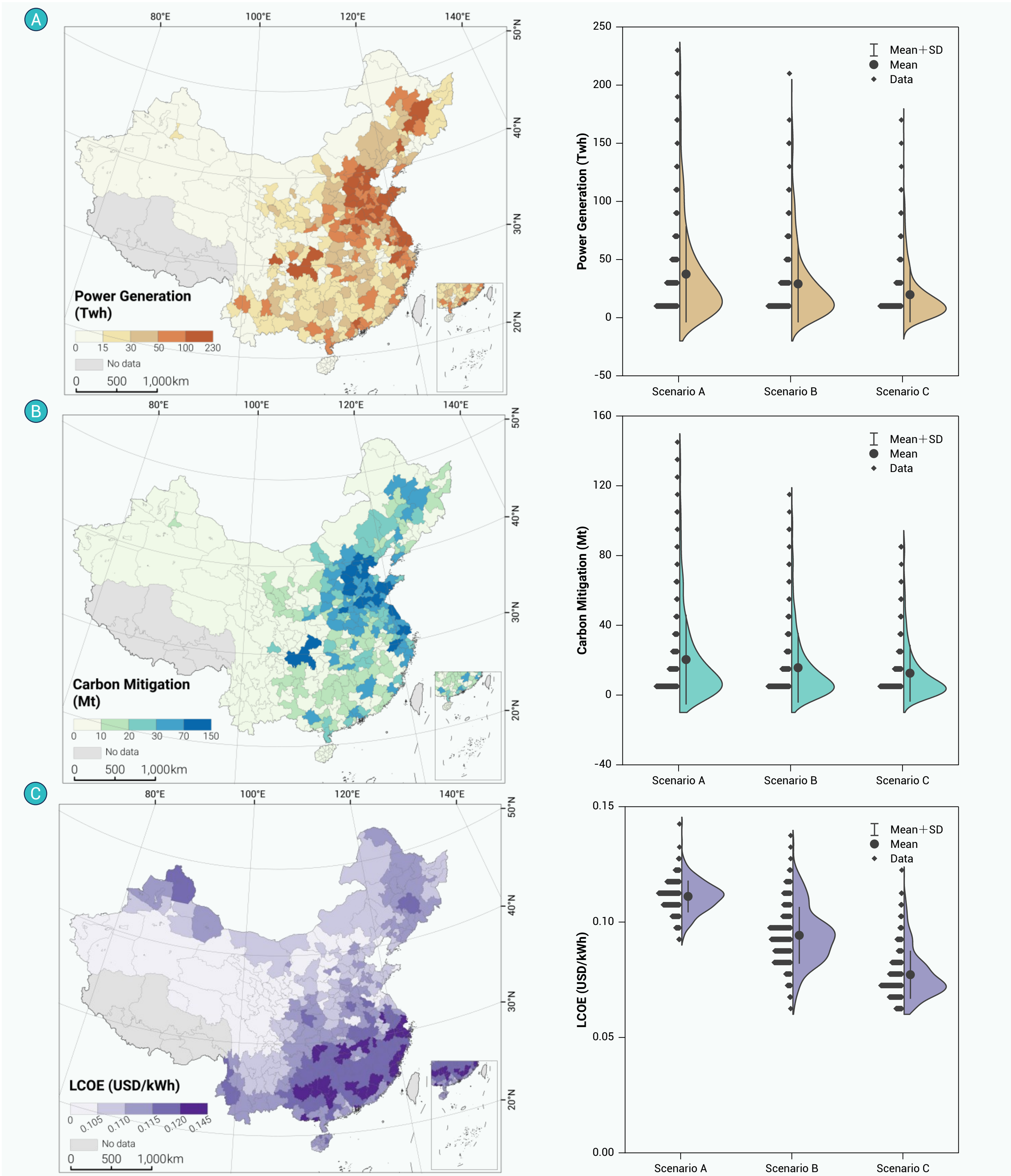

Figure 3. Key indicators for assessing the BIPV potential of 361 prefecture-level cities in China (A) Annual BIPV power generation. (B) Annual BIPV carbon mitigation. (C) Annual BIPV *LCOE*. The left and right sides of the figure represent the aggregated results at the city-level and cluster-level, respectively. Data Credits: All the city administrative boundaries are from the Ministry of Natural Resources, China.

grated 3E assessment framework. The subsequent analysis quantifies this current 3E potential, bridging the gap between theoretical capacity and feasible implementation by simultaneously considering energy output, environmental impacts, and economic viability.

Current BIPV 3E potential

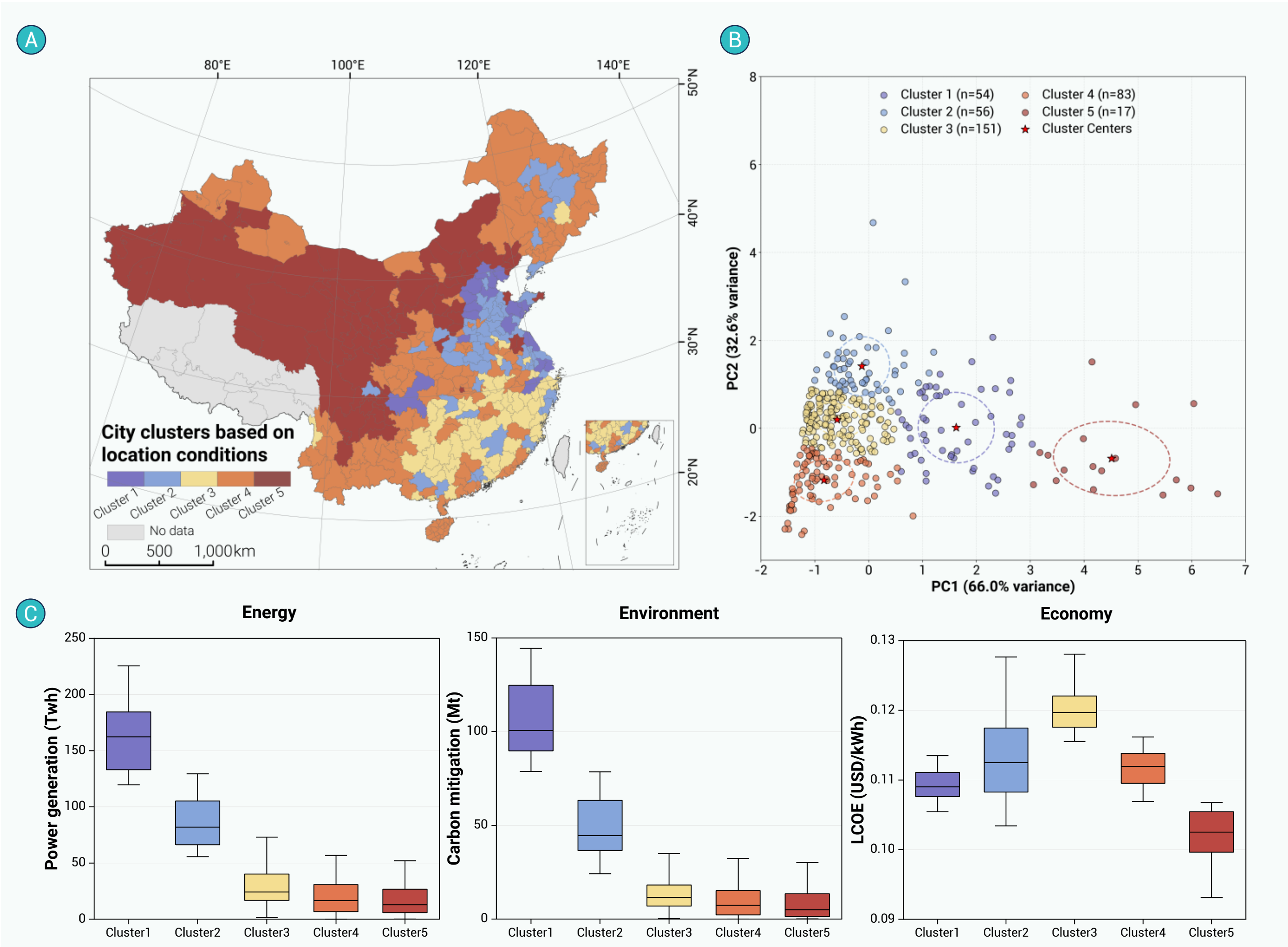

Figure 4. Clustering analysis of cities, based on location conditions that determine the BIPV potential (A) Spatial distribution of cities in each cluster. (B) Principal component analysis (PCA) in each cluster. (C) Location condition characteristics in each cluster in terms of power generation, carbon mitigation, and *LCOE*. Data Credits: All the city administrative boundaries are from the Ministry of Natural Resources, China.

Since BIPV technology is characterized by its ability to cover a diverse range of surfaces in the building envelope, systematic quantification of China's BIPV potential is crucial to the rational development of BIPV. Based on the synergistic 3E perspective, we chose three indicators: power generation, carbon mitigation, and *LCOE* to quantify the BIPV potential (Figure 3). The study indicates that BIPV systems across 361 Chinese prefecture-level cities could generate a total electricity output of 13,518 TWh/yr and achieve a carbon mitigation of 7,359 Mt/yr. The average *LCOE* reached 0.112 USD/kWh. The additional O&M costs for high-rise FIPV increase the LCOE of these systems by about 0.005-0.008 USD/kWh, but this does not alter the overall ranking of clusters or the conclusion that the integrated BIPV system achieves grid parity with coal power. Among them, RIPV systems generate the majority (54%), with FIPV systems contributing the remainder (46%). This underscores the significant role of developing vertical building surface resources in enhancing the energy and environmental benefits of BIPV. The graded statistical map shows that BIPV systems with high energy-environmental potential are concentrated on the southeast side of the Heihe-Tengchong line, indicating that energy conservation and emission reduction potential exhibits a significant spatial coupling characteristic with building area. Meanwhile, BIPV systems with high economic potential are concentrated on the north side, with their distribution showing a significant positive correlation with solar radiation intensity.

To precisely assess the potential of building vertical surface resources, we further analyzed the constraining effects of building height restrictions on BIPV systems, particularly the performance of FIPV. When building heights are limited to 10m and 27m, the energy potential decreases by 22.3% and 38.3%, respectively, while environmental potential decreases by 23.0% and 38.3%, respectively. In cities with high-rise building clusters, the impact of height restrictions on residential buildings is relatively minor because their substantial stock of high-rise buildings has already secured considerable façade resources. The true suppression of potential primarily occurs in commercial districts and planned new urban areas, where the construction of super-tall landmark buildings could have maximized energy output per unit of land area. In terms of economic potential, due to the higher *LCOE* of FIPV, the *LCOE* of BIPV decreases by 13.29% and 28.08%, respectively, under height restrictions. However, this reduction in *LCOE* reflects a decrease in the overall energy output of the system, particularly the loss of high-value façade resources. Under the strict 27m height restriction, although the system's average *LCOE* decreases from 0.112 USD/kWh to 0.080 USD/kWh, the total annual power generation potential is reduced by nearly 40%, meaning cities lose a significant amount of renewable distributed energy resources. Therefore, when formulating urban building height control policies, it is essential to comprehensively balance energy security, economic efficiency, and urban form.

Cluster analysis of the 3E potential

To elucidate the differences in locational conditions determining the BIPV power generation potential, this study conducted intelligent zoning of 361 prefecture-level cities in China using a K-means++ clustering algorithm, with three key evaluation metrics: power generation, carbon mitigation, and *LCOE*.

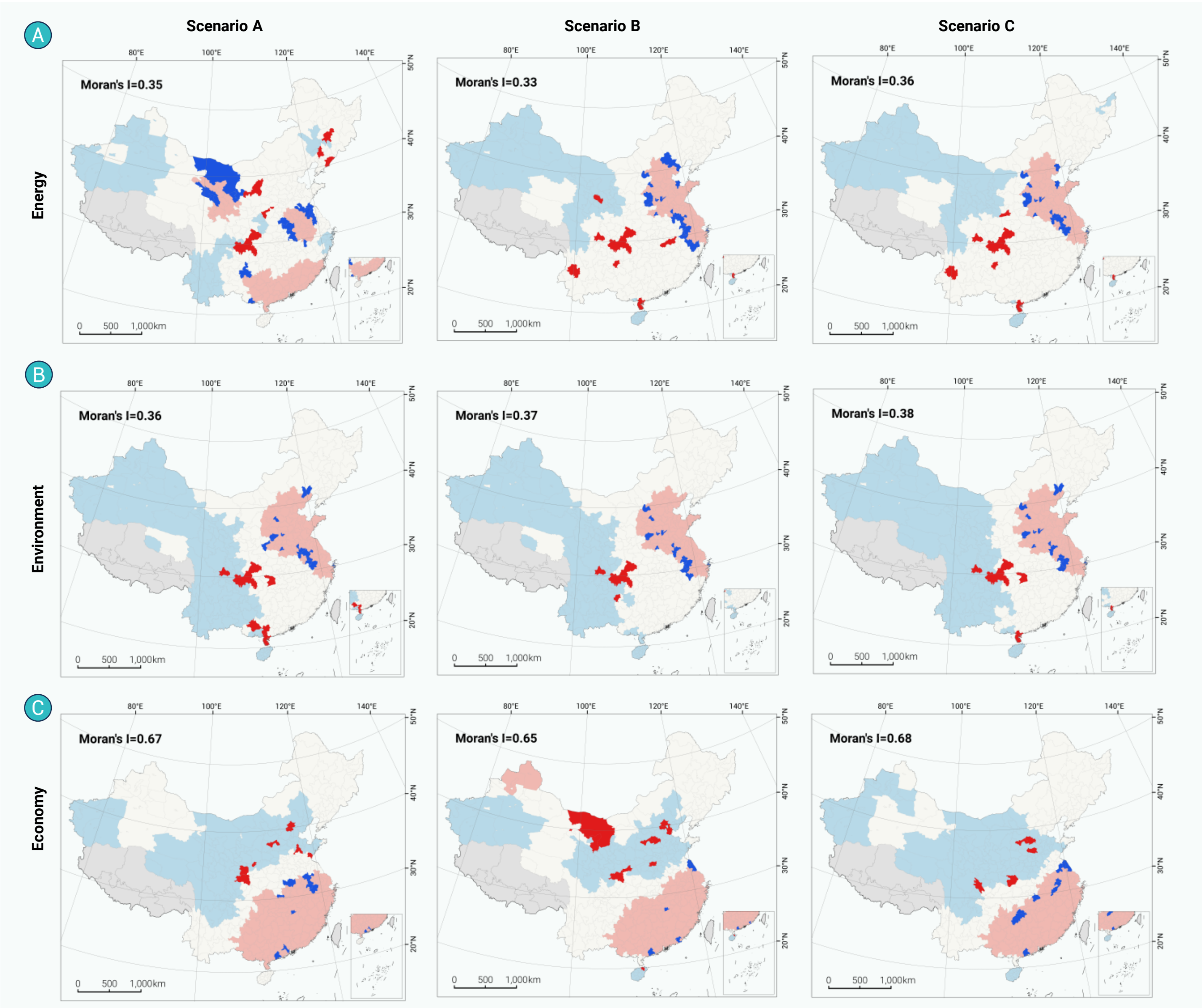

Figure 5. Spatial heterogeneity analysis of the 3E potential of urban BIPV (A) Power generation, (B) Carbon mitigation, and (C) *LCOE*. The figure shows the Local indices of spatial association (LISA) aggregation map. Scenario A considers all buildings, while Scenarios B and C consider buildings over 10m and 27m, respectively. Data Credits: All the city administrative boundaries are from the Ministry of Natural Resources, China.

The optimal cluster number was determined as five groups through silhouette analysis and elbow method,[36,37] effectively deconstructing the spatial hierarchical structure of BIPV resource endowment. Based on the established geographic zoning model, the research further implemented one-way analysis of variance (ANOVA) with multiple comparison tests (Figure 4).[38] All features differed significant differences across different clusters, with large effect sizes ($\eta^2 > 0.5$).

City cluster analysis reveals five distinct patterns, with significant differences in power generation and carbon mitigation effects. Notably, although Cluster 1 and Cluster 2 comprise only 20% of the studied cities, they contribute 55.36% of the total power generation and 60.06% of the total carbon mitigation nationally. This phenomenon is primarily attributed to these clusters possessing dense building agglomerations and high population density. Specifically, all five cities with the highest urban population rankings nationally are located within Cluster 1 and Cluster 2. These cities exhibit high power generation potential, including Shanghai (Cluster 1, 213.46 TWh), Beijing (Cluster 1, 179.81 TWh), and Chengdu (Cluster 2, 179.12 TWh). Their generation potential is generally more than double the national average. However, constrained by lower carbon emission factors, some cities within these clusters demonstrate relatively lower carbon mitigation potential. Cluster 3 contains the largest number of cities. Nevertheless, due to smaller building floor area, its average energy and environmental potential are slightly below the national average. The building surface area of the cities in Cluster 4 are comparable to those in Cluster 3, yet its significantly lower solar radiation levels result in average energy and environmental potentials that are only 70.02% and 66.48% of those of Cluster 3. Cluster 5 covers the largest proportion of the area and generally possesses optimal solar radiation resources. However, due to a severe scarcity of utilizable building area, its average energy potential (17.61 TWh) and environmental potential (9.32 Mt) are the lowest among all clusters.

Economic factors further highlight regional imbalances in urban cluster analysis. Economic analysis reveals that the *LCOE* for BIPV across Chinese cities ranges from 0.093 to 0.143 USD/kWh. Notably, the national average *LCOE* of 0.112 USD/kWh is close to the coal power price (0.118 USD/kWh) and lower than the gas peaking power price (0.169 USD/kWh). This indicates strong economic competitiveness for BIPV that will accelerate its substitution process for coal power. However, it should be noted that the average *LCOE* for FIPV stands at 0.162 USD/kWh, significantly higher than RIPV

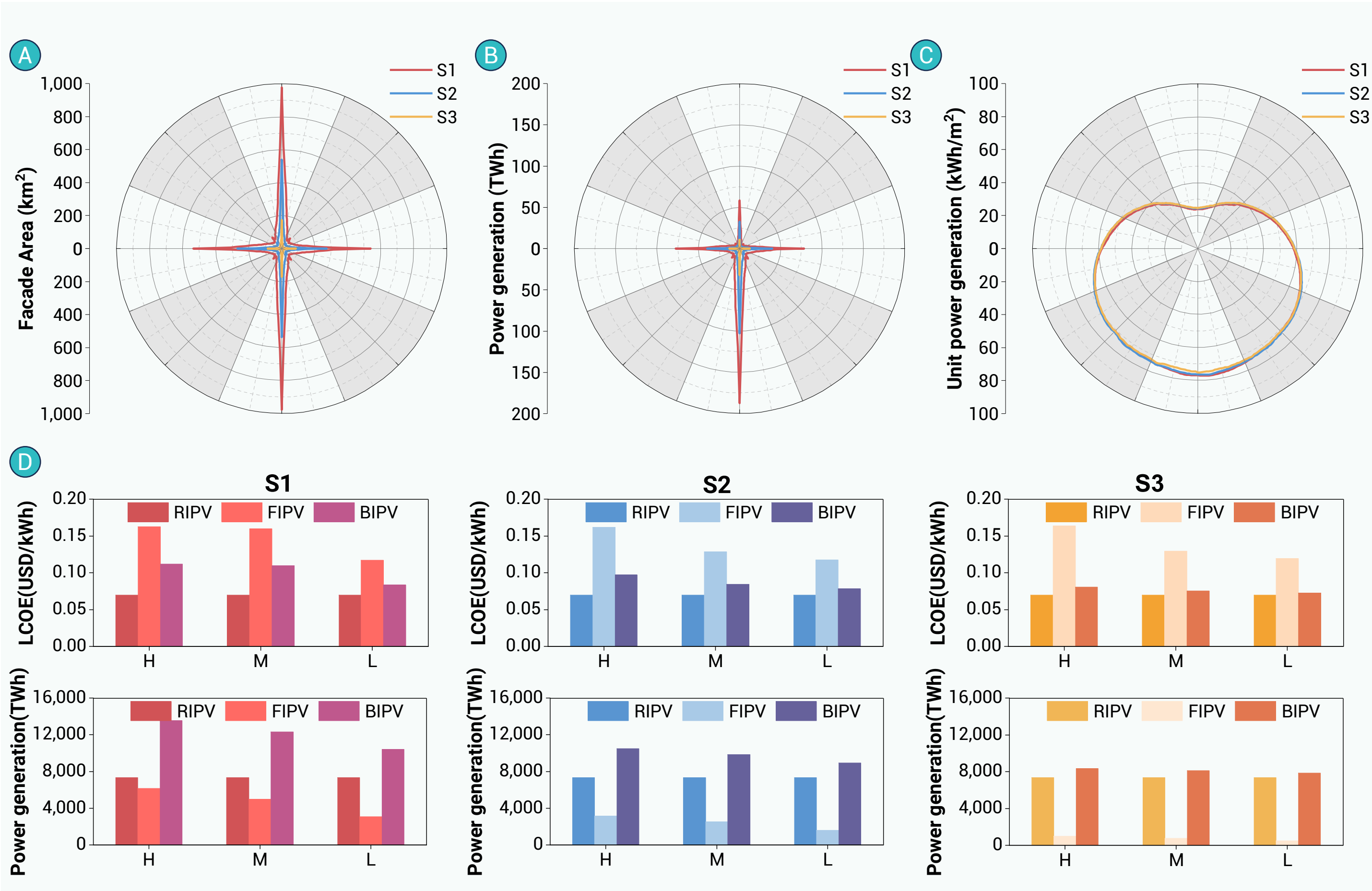

Figure 6. Energy output and economic performance potential of building facades (A) Potential for electricity generation from building facades in China at 1° resolution: facade area, electricity generation, and solar radiation values. (B) Total power generation and *LCOE* of FIPV and BIPV in China under various scenarios.

(0.067 USD/kWh), suggesting FIPV has certain energy and environmental potential, though its economic advantage is less pronounced than that of RIPV. Among the analyzed clusters, Cluster 2 (0.113 USD/kWh) exhibits a slightly higher *LCOE* than the national average, primarily due to the increasing costs caused by the large rooftop installation area proportion. Cluster 1 (0.111 USD/kWh) and Cluster 4 (0.112 USD/kWh) fall slightly below the average, placing them in a moderate position in terms of economic potential. Cluster 3 has the highest *LCOE* (0.121 USD/kWh) with both energy and economic potential below average, suggesting that it should be given low priority for immediate large-scale deployment under current techno-economic conditions. However, as technology costs continue to decline, these cities may become viable in the future; in the interim, cross-regional green power trading offers a more cost-effective pathway for these regions to benefit from renewable energy. Conversely, Cluster 5 achieves the lowest *LCOE* (0.102 USD/kWh), owing to its location in western regions characterized by generally low-rise buildings, resulting in a low facade area proportion, high solar radiation values, and consequently higher PV power generation per unit area. This suggests significant regional variations in BIPV economic performance based on local conditions.

As shown in Figure 3, each cluster exhibits pronounced spatial heterogeneity, with geographically adjacent cities demonstrating similar application potential. The study identifies five distinct potential clusters characterized by significant feature disparities. High-potential clusters (Clusters 1-2), with annual solar radiation intensities approximating the national benchmark (1,481 kWh/m^2), constitute core regions for BIPV deployment. Cluster 1 encompasses 17 prefecture-level cities, including Beijing, Shanghai, and Chongqing. Their average RIPV and FIPV installation areas are 392 km^2 and 558 km^2, respectively, which are about five times the national average, highlighting the scaling advantages of intensive urban development in supercities. Cluster 2 is concentrated in North China, contributing 40% of the nation's total building floor area, reflecting benefits from contiguous regional development. Although Cluster 3 meets radiation thresholds, its comprehensive potential remains constrained by spatial dispersion and building density limitations. Among the low-potential clusters, Cluster 4, which mainly spans cities in South China, exhibits the "double defect" of weak solar radiation intensity (1,324 kWh/m^2) and low usable building surface. Cities in Cluster 5 are predominantly distributed across western regions. Despite possessing the highest radiation levels (1,752 kWh/m^2), their practical developable areas face severe constraints due to sparse building clusters in western plateau areas.

Spatial analysis of the 3E potential

The spatial imbalance of urban-scale PV systems has become a key factor restricting the optimal allocation of resources. At the urban level, there are significant regional differences in solar energy endowment, land availability, and power grid infrastructure, which together lead to spatial variations in the 3E potential of BIPV. To explore the spatial distribution and correlation of key indicators of BIPV systems in Chinese cities, this study employs spatial autocorrelation analysis. Specifically, the global Moran's I is utilized to quantify the degree of spatial clustering or dispersion across the entire study area. This test statistically reveals whether cities with high (or low) values of the key BIPV indicators tend to be located near other cities with similarly high (or low) values, or whether dissimilar values are clustered (Figure 5). The three scenarios in Figure 5 correspond to the height thresholds analyzed in Section 3.2. Scenario A includes all buildings. Scenario B includes buildings above 10m. Scenario C includes buildings above 27m.

Among the 3E parameters, the Moran's I values rank as follows: Economy > Environment ≈ Energy, demonstrating that economic potential exhibits the strongest spatial autocorrelation, followed by environmental potential and energy potential. Analysis of the LISA clustering patterns for the 3E potentials reveals that High-High (H-H) clusters for both energy and environmental potentials are primarily concentrated in Cluster 1 and Cluster 2, while Low-Low (L-L) clusters are mainly found in Cluster 5, presenting a distinct east-west gradient pattern. In contrast, H-H clusters of economic potential are largely aggregated in Cluster 2 and Cluster 5, while L-L clusters are concentrated in Cluster 4, indicating a clear north-south gradient pattern.

To test whether the north-south economic gradient could be an artifact of facade area errors, we performed a robustness check by randomly perturbing the facade area inputs by ±20% and re-calculating *LCOE* and Moran's I. The north-south and east-west gradients remained statistically significant in 96% of the iterations, confirming that this spatial pattern is driven by solar irradiation and electricity tariffs, which are independently measured and highly accurate, rather than by facade area uncertainties.

Economic optimization of BIPV

The introduction of BIPV with relatively poor economic performance may increase the *LCOE* in power systems. For instance, the *LCOE* of FIPV in China typically reaches twice that of RIPV. Nevertheless, the superior power generation potential of FIPV can offset its higher LCOE, thereby improving the project's internal rate of return (IRR), which measures the project's expected annualized profitability, thereby improving its economic viability. For BIPV installations, south-facing facades and rooftops generally demonstrate superior economic performance. Consequently, the installation location is critical to BIPV's economic outcomes; further research is required to quantitatively assess the economic potential across different building orientations (Figure 6).

This study divides the building facade into eight orientations: North (N), Northwest (NW), West (W), Southwest (SW), South (S), Southeast (SE), East (E), and Northeast (NE). As shown in Fig.6, building facade orientations are primarily distributed in the N, W, S, and E. Based on the differences in solar radiation intensity, the facades are further categorized into three gradient zones: high-radiation zones (SW, S, SE); medium-radiation zones (W, E); and low-radiation zones (NW, N, NE). Among these, the solar radiation values in the high-radiation zone exceed 1,000 kWh/m^2, equivalent to about 70% of the average rooftop radiation value (1,528 kWh/m^2).

Given the significant differences in solar radiation intensity across the building facades, this study established three scenarios to compare and analyze the electricity generation and *LCOE* of BIPV systems: H (high + medium + low radiation potential facades), M (high + medium radiation potential facades), and L (high radiation potential facades only). Based on the results of multi-scenario energy potential and economic potential analyses, compared to H, M shows an 8.86% decrease in BIPV total electricity generation and a 2.23% decrease in *LCOE*. For L, the decrease in electricity generation rises to 22.96%, but the *LCOE* drops significantly by 25.53% to 0.08 USD/kWh. Analysis of BIPV potential across cities shows that as the selection criteria for facade solar radiation potential become stricter, the potential of each city shifts toward the lower-left corner in the scatter plot, indicating that while electricity generation decreases, economic viability improves. Notably, in scenario L, the system's maximum potential electricity generation decreases from 13,518 TWh to 10,414 TWh. Considering both electricity generation and cost-effectiveness, the M significantly improves economic viability while maintaining the total electricity generation scale of the H, thereby offering superior comprehensive benefits for future development.

DISCUSSION

National BIPV potential and deployment economics

The total BIPV generation potential of 13,518 TWh estimated in this study is sufficient to meet China's annual electricity demand. More importantly, facades contribute substantially to this potential. The available installation area on building facades is 1.45 times that of rooftops, and FIPV accounts for approximately 40% of the total carbon mitigation. Even under conservative height constraints (10 m and 27 m thresholds), FIPV still increases total generation by 42.8% and 13.4% respectively. These findings demonstrate that facades are not a marginal supplement but a central component of urban BIPV deployment. Previous studies that focused only on rooftops have systematically underestimated the true solar potential of Chinese cities by overlooking vertical surfaces. The inclusion of facades fundamentally changes the scale of what is technically achievable.

Although the *LCOE* of FIPV alone is 2.4 times higher than that of RIPV, the integrated system achieves economic viability through two mechanisms. First, the combined generation from rooftops and facades smooths the daily output profile because east-facing facades generate more in the morning, south-facing facades peak at midday, and west-facing facades produce in the afternoon. These better matches building electricity load curves and reduces reliance on storage. Second, not all facades need to be deployed at once. Our scenario analysis shows that focusing only on south-facing facades and rooftops reduces the *LCOE* by 30% compared to deploying all facades, while retaining 77% of total generation. The intermediate M scenario (excluding only north-facing facades) sacrifices only 8.9% of generation but lowers *LCOE* by 2.2%. These trade-offs provide a clear staged deployment strategy: prioritize south-facing facades for immediate grid parity, then incorporate east and west facades as technology costs decline. Nationally, the average BIPV *LCOE* of 0.112 USD/kWh is already competitive with coal power at 0.118 USD/kWh, indicating that further cost reductions will accelerate substitution.

Spatial heterogeneity and differentiated urban strategies

The spatial analysis reveals two distinct gradients. Energy and environmental potentials both follow an east-west gradient, driven primarily by building density. The densely urbanized regions south of the Heihe-Tengchong Line, despite having only moderate solar radiation, dominate total generation because of their vast building stocks. In contrast, economic potential follows a north-south gradient, driven by solar radiation and electricity tariffs. Northern and western regions have higher irradiation and thus lower LCOE, even though their total building area is smaller.

About 60% of the national generation and carbon reduction potential is concentrated in just 20% of cities. This concentration calls for differentiated strategies rather than a uniform national policy. For high-potential clusters (Clusters 1 and 2), large-scale deployment should be prioritized, supported by carbon trading markets to monetize emission reductions. For building-rich but low-radiation cities like Chongqing, targeted FIPV subsidies can help overcome the economic disadvantage. For high-radiation but building-scarce regions like Cluster 5, agrivoltaics offers a land-efficient alternative to ground-mounted PV.

For low-radiation and low-potential regions (Clusters 3 and 4), cross-regional green power trading is more practical than local deployment. For Cluster 3, which exhibits the lowest combined 3E performance, we do not recommend prohibiting BIPV deployment entirely. Instead, we advocate a "wait-and-see" strategy: avoiding large subsidies for local deployment, while promoting participation in national green power markets. This allows these cities to benefit from renewable energy without incurring the high costs of local installation. As BIPV capital costs continue to decline, these regions may become economically viable for local deployment in the longer term.

Implementation barriers and limitations

Our 2.5D extrusion method inevitably simplifies building geometries by ignoring setbacks, balconies, and curved facades, resulting in a 23% mean absolute percentage error in total facade area. Nevertheless, the Spearman correlation of 0.91 confirms that relative rankings across cities are highly reliable, which is the primary objective of this national-scale screening. Shading presents another challenge. While we do not perform dynamic ray-tracing, shading effects are incorporated through aggregated factors: the 40% facade usability factor and the 0.8 performance ratio embed deductions for mutual building shading and partial shading losses. PVSYST simulations for six representative cities indicate that shading reduces annual generation by approximately 15-20%, consistent with these deductions. Although this simplified treatment may overestimate generation in dense urban cores, the relative ranking across cities remains robust. The Monte Carlo uncertainty analysis, which varies PR across the 0.75-0.85 range as shown in Supplementary Table S4, yields a 90% confidence interval of 10,600 to 16,200 TWh/yr, capturing the combined effects of geometric simplification, shading, and regional soiling differences. Future city-scale assessments should integrate the PV_LIB shading module or similar dynamic ray-tracing tools once high-resolution 3D city models become available, enabling more precise absolute estimates for project-level design.

Another source of technical uncertainty arises from the distinct performance characteristics of rooftop and facade PV systems. These two system types differ substantially in tilt angle, orientation, ventilation conditions, operating temperatures, and soiling rates. In our analysis, we have explicitly distinguished these parameters. Module efficiency is set at 20% for RIPV and 15% for FIPV, and the performance ratio is slightly lower for FIPV at 0.78 than for RIPV at 0.80. This difference accounts for higher operating temperatures due to limited natural convection behind vertical surfaces and increased soiling near ground level. To test the sensitivity of our conclusions to these differentiated assumptions, we varied FIPV efficiency from 13% to 18% and FIPV performance ratio from 0.75 to 0.85 in our Monte Carlo and sensitivity analyses as detailed in Supplementary Tables S4 and S5. The results show that the national average *LCOE* changes by only ±4% across this range. Furthermore, the 30% LCOE reduction for the optimised scenario that prioritises south-facing facades and rooftops persists across all tested parameter combinations. This confirms that while RIPV and FIPV parameters differ in practice, our core findings regarding the added value of facades and the economic benefits of orientation-specific deployment remain robust.

Beyond technical uncertainties, real-world economic and institutional barriers further reduce achievable potential. For ownership fragmentation in multi-owner buildings, we conservatively assume that only 50% of residential high-rises, which constitute approximately 65% of building stock in Clusters 1 and 2, can reach installation agreements via homeowners' associations or ESCO models, while 90% of single-owner commercial buildings are adoptable. This leads to a national loss of approximately 18-22%. By overlaying national-level historic protection zones, which cover about 2.8% of urban built-up area, we estimate that heritage and aesthetic restrictions reduce potential by an additional 3-5%. A cluster-specific impact matrix is provided in Supplementary Table S6. Despite these barriers, our economic conclusions remain robust: *LCOE* is a per-kWh metric that scales linearly with area, and systematic multiplicative errors affect generation and installation costs proportionally, leaving *LCOE* largely unchanged. The north-south economic gradient is driven by independently measured solar irradiation and electricity tariffs rather than by facade area errors.

Urban planning constraints also merit consideration. Height thresholds of 10m and 27m were applied to reflect practical installation feasibility, with low-rise buildings allowing ladder access, mid-rise buildings requiring scaffolding, and high-rise buildings demanding suspended platforms, as well as to account for shading effects from taller structures. Vegetation shading is neglected due to data limitations, which may modestly overestimate generation in low-rise residential areas with dense street trees. Future research should extend this static assessment by incorporating urban expansion scenarios and building stock turnover projections, which are not modelled in the present study but are critical for long-term BIPV planning. As urbanisation and high-rise construction continue to reshape city morphologies, dynamic growth projections will be essential to refine BIPV potential estimates over longer planning horizons.

CONCLUSION

This study provides a unified city-scale BIPV assessment framework covering 361 Chinese cities, integrating building footprints, height, orientation, rooftop and facade areas, solar irradiation, carbon emission factors, and *LCOE* parameters. The estimated annual generation potential is 13,518 TWh (median), with a 90% confidence interval of 10,600 to 16,200 TWh derived from the Monte Carlo uncertainty analysis. FIPV increases total generation by up to 60% compared to rooftop-only systems. Focusing on south-facing facades and rooftops reduces *LCOE* by 30% relative to deploying all facades, offering a clear near-term strategy.

Spatially, energy and environmental potential follow an east-west gradient driven by building density, while economic potential follows a north-south gradient driven by solar irradiation. About 60% of generation potential is concentrated in 20% of cities, calling for differentiated policies ranging from large-scale deployment in high-potential clusters to green power trading in low-potential regions.

Future research should integrate high-resolution 3D city models, dynamic shading simulation, heritage mapping, and region-specific soiling rates. For building-scarce but high-radiation regions like Cluster 5, agrivoltaics offers a land-efficient alternative. Policy development should address ownership fragmentation, aesthetic barriers, and heritage restrictions while leveraging urbanization and technological advancements to fully realize BIPV's role in China's carbon-neutral future.

REFERENCES

1. Ding C., Ke J., Levine M., et al. (2024). Potential of artificial intelligence in reducing energy and carbon emissions of commercial buildings at scale. *Nat. Commun.* **15**:5916. DOI:10.1038/s41467-024-50088-4
2. Bai X. and Shi P. (2025). China's urbanization at a turning point-challenges and opportunities. *Science* **388**:3443. DOI:10.1126/science.adw3443
3. Jun K., Seungkeun Y. and Taehoon H. (2025). Analyzing the cooling effect, thermal comfort, and energy consumption of integrated arrangement of high-rise buildings and green spaces on urban heat island. *Sustain. Cities Soc.* **119**:106105. DOI:10.1016/j.scs.2024.106105
4. Ma M. Zhang S., Liu J., et al. (2025). Building floorspace and stock measurement: A review of global efforts, knowledge gaps, and research priorities. *Nexus* **2**:100075. DOI:10.1016/j.ynexs.2025.100075
5. Cai W., Yu Y., and Liu Y. (2025). Research Report on Carbon Emission in Urban and Rural Construction in China. *Architecture* **2**:56–63.
6. Gherghina M., Dokshin F. A., and Leffel B. (2025). Unequal solar photovoltaic performance by race and income partly reflects financing models and installer choices. *Nat. Energy* **10**:697–706. DOI:10.1038/s41560-025-01743-7
7. Wang Y., Wang R., Tanaka K., et al. (2023). Accelerating the energy transition towards photovoltaic and wind in China. *Nature* **619**:761–767. DOI:10.1038/s41586-023-06180-8
8. . International Energy Agency. (2026). Snapshot of Global PV Markets 2026. *IEA*.
9. Zhao Y., Li S., Yang D., et al. (2024). Assessment of site suitability for centralized photovoltaic power stations in Northwest China's six provinces. *J. Environ. Manage.* **366**:121820. DOI:10.1016/j.jenvman.2024.121820
10. Ballif C., Perret-Aebi L.-E., Lufkin S., et al. (2018). Integrated thinking for photovoltaics in buildings. *Nat. Energy* **3**:438–442. DOI:10.1038/s41560-018-0176-2
11. Li F., Dong W. and Wu W. (2023). A general model for comprehensive electrical characterization of photovoltaics under partial shaded conditions. *Adv. Appl. Energy* **9**:100118. DOI:10.1016/j.adapen.2022.100118
12. . China Construction Association. (2025). Statistical analysis of the development of the construction industry 2024. *CCA*.
13. Zhao K. and Gou Z. (2023). Influence of urban morphology on facade solar potential in mixed-use neighborhoods: Block prototypes and design benchmark. *Energy and Build.* **297**:113446. DOI:10.1016/j.enbuild.2023.113446
14. Liang H., Shen J., Yip H.L., et al. (2024). Unleashing the green potential: Assessing Hong Kong's building solar PV capacity. *Appl. Energy* **369**:123567. DOI:10.1016/j.apenergy.2024.123567
15. . Yu Z., Lu Z., Xin W., et al. (2024). Environmental and economic evaluation of urban building-integrated photovoltaic and electric vehicle system. *J. Build. Eng.* **95**:110205. DOI10.1016/j.jobe.2024.110205.
16. Zhang Z., Qian Z., Chen M., et al. (2025). Worldwide rooftop photovoltaic electricity generation may mitigate global warming. *Nat. Clim. Change* **13**:101. DOI:10.1038/s41558-025-02276-3
17. Khan A., Khorat S., Khatum R., et al. (2024). Rooftop photovoltaic solar panels warm up and cool down cities. *Nat. Cities* **1**:780–790. DOI:10.21203/rs.3.rs-3485787/v1
18. Zhang S. and Chen W. (2022). Assessing the energy transition in China towards carbon neutrality with a probabilistic framework. *Nat. Commun.* **13**:87. DOI:10.1038/s41467-021-27671-0
19. Isik M., Dodder R. and Kaplan P. O. (2021). Transportation emissions scenarios for New York City under different carbon intensities of electricity and electric vehicle adoption rates. *Nat. Energy* **6**:92–104. DOI:10.1038/s41560-020-00740-2
20. Li Z. and Hu D. (2022). Exploring the relationship between the 2D/3D architectural morphology and urban land surface temperature based on a boosted regression tree: A case study of Beijing, China. *Sustain. Cities Soc.* **78**:103392. DOI:10.1016/j.scs.2021.103392
21. Song Z., Cao S. and Yang, H. (2023). Assessment of solar radiation resource and photovoltaic power potential across China based on optimized interpretable machine learning model and GIS-based approaches. *Appl. Energy* **339**:121005. DOI:10.1016/j.apenergy.2023.121005
22. Xu H. and Yang, R. (2025). The impact of water rights reform on economic development: Evidence from city-level panel data in China. *J. Environ. Manag* **374**:124082. DOI:10.1016/j.jenvman.2025.124082
23. Vroon T., Teunissen E., Drent,M., et al. (2021). Escaping the niche market: An innovation system analysis of the Dutch building integrated photovoltaics (BIPV) sector. *Renew. Sustain. Energy Rev.* **155**:111912. DOI:10.1016/j.rser.2021.111912
24. Saretta E., Caputo P. and Frontini F. (2020). An integrated 3D GIS-based method for estimating the urban potential of BIPV retrofit of façades. *Sustain. Cities Soc.* **62**:102410. DOI:10.1016/j.scs.2020.102410
25. Dong K., Yu Q., Guo Z., et al. (2025). Advancing building facade solar potential assessment through AIoT, GIS, and meteorology synergy. *Adv. Appl. Energy*

17:100212. DOI:10.1016/j.adapen.2025.100212
26. Lu Y., Ju X. and Zhang L. (2019). Rapid estimation method for the installation area of building photovoltaic systems in the early design stage (in Chinese). *Construct. Sci. Tech.* 2:58–62.
27. Feng X., Ma T., Yamaguchi Y., et al. (2022). Potential of residential building integrated photovoltaic systems in different regions of China. *J. Build. Eng.* 58:105077. DOI:10.1016/j.esd.2022.11.006
28. . Che Y., Li X., Liu X., et al. (2025). 3D-GloBFP: the first global three-dimensional building footprint dataset. *Zenodo.* DOI:10.5281/zenodo.15487006
29. Jin Y., Hu S., Ziegler A. D., et al. (2023). Energy production and water savings from floating solar photovoltaics on global reservoirs. *Nat. Sustain.* 6:865–874. DOI:10.1038/s41893-023-01089-6
30. . Ministry of Housing and Urban-Rural Development of China. (2011). Residential building design code (GB 50096-2011). *China Architecture & Building Press.*
31. . Ministry of Housing and Urban-Rural Development of China. (2019). Unified standard for civil building design (GB 50352-2019). *China Architecture & Building Press.*
32. Wang Y., Mauree D., Sun Q., et al. (2020). A review of approaches to low-carbon transition of high-rise residential buildings in China. *Renew Sustain Energy Rev.* 131:109990. DOI:10.1016/j.rser.2020.109990
33. Chen Y. (2023). Spatial autocorrelation equation based on Moran's index. *Sci Rep* 13:19296. DOI:10.1038/s41598-023-45947-x
34. Zhao Z., Li H. and Wang, S. (2022). Identification of the key design parameters of Zero/low energy buildings and the impacts of climate and building morphology. *Appl. Energy* 328:120185. DOI:10.1016/j.apenergy.2022.120185
35. Yu Z., Chen C., Lou D., et al. (2025). Energy-economy-environment evaluation of building-integrated photovoltaic considering facade factors for representative megacities in China. *Appl. Energy* 389:125839. DOI:10.1016/j.apenergy.2025.125839
36. Yang L., Yang Y., Shen Y., et al. (2024). Urban development pattern's influence on extreme rainfall occurrences. *Nat. Commun.* 15:3997. DOI:10.1038/s41467-024-48533-5
37. Eyre R., De Luca F. and Simini F. (2020). Social media usage reveals recovery of small businesses after natural hazard events. *Nat. Commun.* 11:1629. DOI:10.1038/s41467-020-15405-7
38. Zhang Y., Shi K., Woolway R.I., et al. (2025). Climate warming and heatwaves accelerate global lake deoxygenation. *Sci. Adv.* 11:5369. DOI:10.1126/sciadv.adt5369

FUNDING AND ACKNOWLEDGMENTS

We appreciate the financial supports from the National Natural Science Foundation of China (Nos. 72573075, 72173058 & 72394391), High-level University Special Fund (G030290001) and supports from the State Key Laboratory of Soil Pollution Control and Safety, Southern University of Science and Technology.

AUTHOR CONTRIBUTIONS

All authors contributed to the manuscript and approved the final version.

DECLARATION OF INTERESTS

The authors declare no competing interests.

DATA AND CODE AVAILABILITY

Data are available from the corresponding author upon reasonable request.

SUPPLEMENTAL INFORMATION

It can be found online at: https://doi.org/10.59717/j.xinn-energy.2026.100179